



## CORRECTING THE TOPOGRAPHIC EFFECT ON SPOT-6/7 MULTISPECTRAL IMAGERIES: A COMPARISON OF DIFFERENT DIGITAL ELEVATION MODELS

Zylshal ZYLSHAL<sup>1\*</sup> , Athar Abdurrahman BAYANUDDIN<sup>1</sup> , Ferman Setia NUGROHO<sup>1</sup> ,  
Sutan Takdir Ali MUNAWAR<sup>1</sup> 

DOI : 10.21163/GT\_2021.163.13

### ABSTRACT :

The topographic effect on satellite imagery has long been acknowledged and several methods have been proposed to address it. These methods mostly employ a digital elevation model to identify topographic conditions. The availability of various digital elevation models (DEMs) with different spatial resolutions prompts a thorough investigation to select suitable data for use when correcting the topographic effect on high-resolution satellite imagery. The release of Digital Elevation Model Nasional (DEMNAS) with its 8-meter spatial resolution provides a similar spatial resolution with SPOT-6/7 multispectral data (6 meters). This study presents our results for topographic correction performed using three different DEMs on orthorectified SPOT-6/7 multispectral data. These DEMs are Shuttle Radar Topography Mission (SRTM) and ALOS World 3D 30 meters (AW3D30), as well as DEMNAS. All three DEMs were resampled to match SPOT-6/7 spatial resolution (6 meters). Atmospheric correction using the MODTRAN-4 algorithm was conducted on the SPOT-6/7 multispectral images. Our study was conducted on two test sites located in the mountainous region over South Sulawesi Province, Indonesia. The Minnaert correction was chosen as the correction algorithm with the  $k$  constant calculated for each band over forest land cover. To evaluate the performance of each DEM, visual evaluation and statistical assessment were employed. Pixel values before and after topographic correction were compared over sunlit as well as shaded forest. Coefficient of variation (CV) was used as the statistical assessment tool. Our results show that AW3D30 is able to reduce the topographic effect on SPOT-6/7 multispectral images. The correlation ( $r$ ) between image surface reflectance value and local illumination were reduced from 0.78 to -0.06 for the best performer on the NIR infrared band. CV was also reduced from 24.46 to 19.02 for the same NIR band. AW3D30 performed the best without the apparent under- and over-correction produced by the two other DEMs. Tweaks and modifications are found to be necessary to resolve the under-correction encountered when using SRTM and the over-correction associated with using DEMNAS on SPOT-6/7 multispectral imagery.

**Key-words:** AW3D30, DEMNAS, SRTM, Minnaert correction, SPOT-6, SPOT-7

## 1. INTRODUCTION

Recent advances in Earth observation (EO) satellite technology have seen improved spatial resolution in produced imagery. While high-spatial-resolution satellite images can offer greater detail, they are still affected by the environment. The topographic variation of mountainous regions often causes different spectral radiance to the satellite imagery. The combination of terrain's slope and aspect with solar zenith and azimuth angles often causes radiometric distortion (Holben & Justice, 1980). A sun-facing slope appears brighter than a slope facing away from the sun and for homogenous land cover such as forest this can cause a distinctly different reflectance value, potentially leading to misclassification of land cover.

While topographic correction has mainly been investigated for medium-spatial-resolution images, such as those produced by Landsat (Justice, Wharton & Holben, 1981; Kawata, Ueno & Kusaka, 1988; Leprieur, Durand & Peyron, 1988; Civco, 1989; Gu & Gillespie, 1998; Riaño *et al.*,

---

<sup>1</sup>Indonesian National Institute of Aeronautics and Space (LAPAN), Remote Sensing Technology and Data Center, 17310, Jakarta, Indonesia, \*[zylshal@lapan.go.id](mailto:zylshal@lapan.go.id), [athar.abdurrahmanb@lapan.go.id](mailto:athar.abdurrahmanb@lapan.go.id), [fermansetia@gmail.com](mailto:fermansetia@gmail.com), [sta.munawar@lapan.go.id](mailto:sta.munawar@lapan.go.id)

2003; Gao & Zhang, 2009b; Li, Im & Beier, 2013; Vanonckelen *et al.*, 2014; Vázquez-Jiménez *et al.*, 2017), SPOT 5 (Richter, Kellenberger & Kaufmann, 2009), and Sentinel-2 (Chen *et al.*, 2020), high-spatial-resolution imagery also suffers from topographically-induced illumination variation (Law & Nichol, 2004). Thus, topographic correction of high-spatial-resolution satellite images remains essential. Simple band rationing can reduce the spectral discrepancies caused by varying slope aspect (Chavez Jr., 1996). However, this approach comes with consequent reduced radiometric resolution of the data itself. Another method is to use digital elevation model (DEM) data. By using DEMs, the terrain's slope, aspect, inclination to the sun and the satellite's sensor can be modeled.

Several studies have been conducted to find out how different DEMs affect topographic correction results. These studies can generally be categorized into two groups: those using medium-resolution EO satellite data, such as Landsat MSS (Justice, Wharton & Holben, 1981), Landsat-7 ETM+ (Gao & Zhang, 2009b), Landsat-8 OLI (Wu, Jin & Fan, 2016; Pimple *et al.*, 2017; Umarhadi & Danoedoro, 2019), SPOT-4 (Shepherd & Dymond, 2003), and LAPAN-A3 (Zylshal, 2019); and those using high-resolution EO satellite data, such as Quickbird (Wu *et al.*, 2008) and IKONOS (Nichol & Hang, 2013). Correction of topographic effects on medium-resolution data has been extensively studied using globally available DEM data, such as Shuttle Radar Topographic Mission (SRTM), ALOS World 3D DEM (AW3D30), and ASTER GDEM. These DEMs perform well when combined with EO satellite imagery of relatively comparable spatial resolution.

Several studies suggest using comparable spatial resolution of DEM and satellite imagery to achieve the best topographic correction (Kawata, Ueno & Kusaka, 1988; Goyal, Seyfried & O'Neill, 1998; Hantson & Chuvieco, 2011; Pimple *et al.*, 2017). On the other hand, the use of DEM spatial resolution that is relatively coarser than the EO imagery has also have been proven to be able to produce topographically corrected images (Riaño *et al.*, 2003; Richter, Kellenberger & Kaufmann, 2009; Goslee, 2012; Nichol & Hang, 2013). Another problem is the availability of this type of high-resolution DEM data. Typical high-spatial-resolution DEM data such as Light Detection and Ranging (LiDAR) and Airborne Interferometric Synthetic Aperture Radar (IfSAR) is still not fully available for many rural areas in developing countries (Nkwunonwo, Whitworth & Baily, 2020). Fortunately, for the Indonesian region a nationwide high-resolution DEM known as DEM Nasional (DEMNAS) was released for general use in 2018 (BIG, 2018). Two initial studies have been conducted into how well DEMNAS performs in terms of topographic correction (Umarhadi & Danoedoro, 2019; Zylshal, 2019). Results of these studies indicate that topographic correction performed using DEMNAS as the elevation data can subdue topographic effects on EO satellite imagery. Both of these studies, however, tested DEMNAS on medium-spatial-resolution imagery (Landsat and LAPAN-A3). How well it performs on high-spatial-resolution data such as SPOT-6/7 is still unknown. The 8-meter spatial resolution of DEMNAS (BIG, 2018; Julzarika & Durdjani, 2019) is the closest DEM data to the 6-meter multispectral imagery provided by SPOT-6/7.

The SPOT-6 and SPOT-7 constellation is composed of twin satellites operating as a true constellation on the same orbit and phased 180° from each other (referred to throughout this paper as SPOT-6/7). Its large swath combined with its high spatial resolution have proven it to be useful as a monitoring tool that can provide cloud-free imagery over a wide area (Nonin *et al.*, 2013). Its ability to monitor forest areas (Li *et al.*, 2015) and to estimate the above-ground biomass of such forest (Motlagh *et al.*, 2018; Hlatshwayo *et al.*, 2019; Nguyen & Kappas, 2020) gives SPOT-6/7 an important role in efforts to ensure global food security and combat land degradation. With its plan to be in service until 2024 (Nonin *et al.*, 2013), and considering its usefulness, a reference for the most suitable approach and DEM source for topographic correction of SPOT-6/7 imagery is essential. Information about the use of topographic correction on SPOT-6/7 imagery is, however, still limited. A previous study utilizing SCS+C combined with SRTM data showed that topographic correction can improve classification accuracy for SPOT-6/7 images (Rani *et al.*, 2017). However, that research solely used classification accuracy as the evaluator, whereas classification accuracy is actually determined by many factors, including classification algorithm, sample size, and class covariance (Fan *et al.*, 2018; Zylshal, 2020). It is our view that further investigation into SPOT-6/7 topographic correction is still needed.

To understand how well the topographic correction is performed, two well-known, globally available DEMs, namely the 3 arc second SRTM as well as the ALOS World 3D 30 meter (AW3D30) were also investigated. The use of DEMNAS and AW3D30 for specific topographic correction of SPOT-6/7 imagery has never been published before. By using these DEMs with varying spatial resolutions, the objective of this research is to investigate what is the best DEM for topographic correction of SPOT-6/7 imagery. Using the Minnaert correction algorithm on two different test sites, we attempt to investigate how well these DEMs perform on SPOT-6/7 imagery. Our study will be the first to use DEMNAS and AW3D30 as DEM data applied to SPOT-6/7 imagery. The results of this study will advance our understanding of how to appropriately select the DEM to reduce topographic effects on SPOT-6/7 data over mountainous regions.

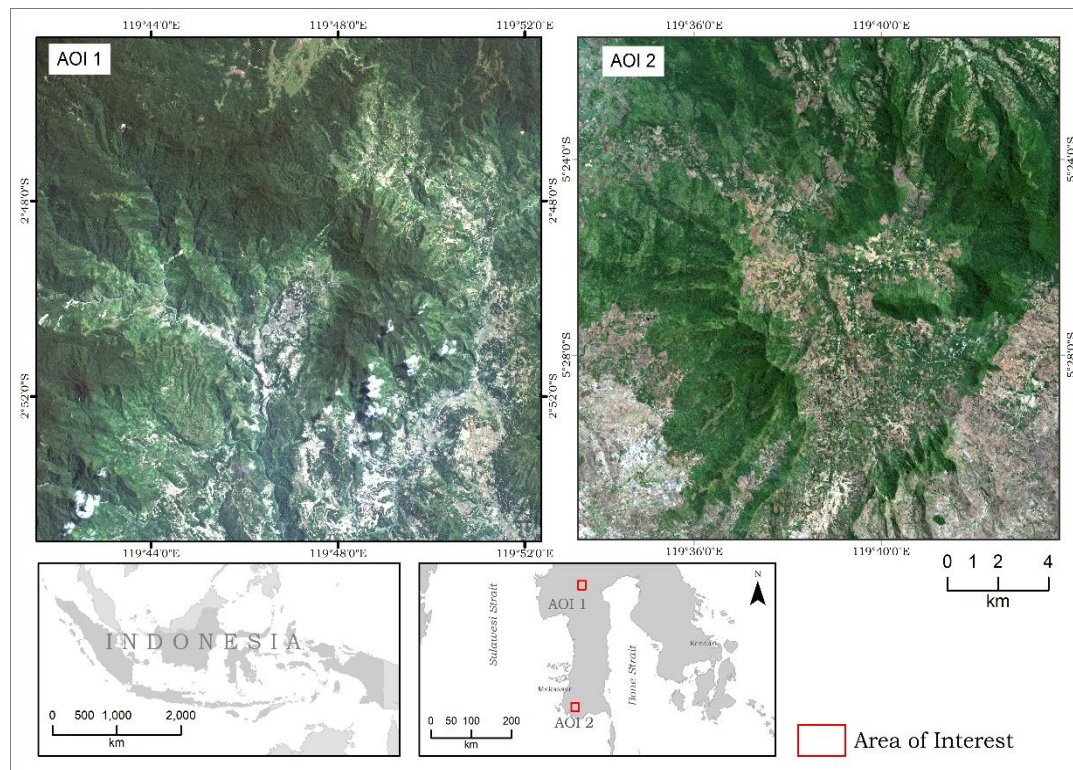


**Fig. 1.** The test site for topographic correction over the Sulawesi region shown in red–green–blue (RGB) composite images from SPOT-6/7. The left-hand image, AOI1, is over the North Toraja region while the image on the right, AOI2, is over the Gowa region.

## 2. STUDY AREA

We chose two test sites, both located in the South Sulawesi region of Indonesia. Each test site is  $23 \times 23$  km wide (**Fig. 1**). Test site 1 (AOI 1) is located in the northern part of the South Sulawesi region. The terrain is oriented in all directions and is dominated by hilly and mountainous relief, with slopes ranging from 0 to 87 degrees. Based on the global land-cover map produced by Copernicus, land cover is mainly forest, herbaceous vegetation, and cropland. AOI 1 is comprised of two landform types. Karst formations cover a small portion of the southeastern part, with volcanic landforms dominating the rest of the site. Test site 2 (AOI 2) is located in the southern part of the South Sulawesi region on an ancient volcanic landform comprising the Baturappe-Cindakko volcanic formation (Tpbv). The terrain is oriented in all directions and dominated by hilly and mountainous relief. The relief undulates with slopes ranging from 0 to 69 degrees (**Fig. 2**). Based on the global land-cover map produced by Copernicus, the dominant land cover at this site is closed forest and cropland.



Climatic conditions at the two sites differ slightly, with AOI 2 being generally drier than AOI 2. As shown in **Fig. 1**, there is an obvious difference in green vegetation coverage between the two sites, even though both data sets are taken during the same season. More detailed information on the imagery used is discussed later in this paper.

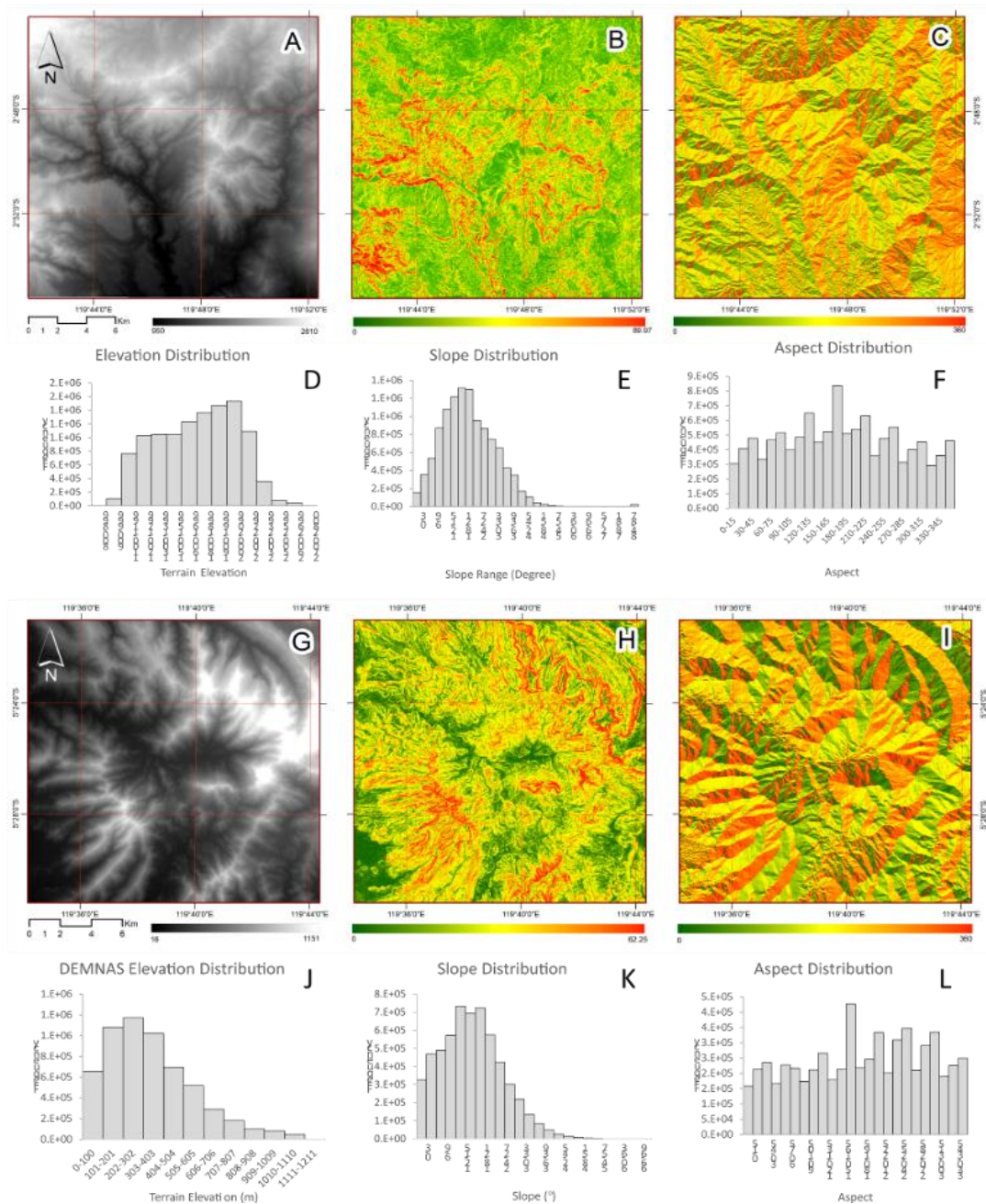


**Fig. 2.** Terrain conditions in the study area derived from DEMNAS data: (A) elevation map for AOI 1; (B) slope map for AOI 1; (C) aspect map for AOI 1; (D), (E), and (F) distributions for elevation, slope, and aspect, respectively; (G) elevation map for AOI 2; (H) slope map for AOI 2; (I) aspect map for AOI 2; (J), (K), and (L) show distributions of elevation, slope, and aspect, respectively.

### 3. DATA AND METHODS

#### 3.1. Digital elevation model (DEM)

**Fig. 2** shows the DEMs used in this study. SRTM was launched in 2000, and with its global coverage and free-of-charge distribution system, has become one of the most-used sources of DEM data for topographic correction (Vincini & Frazzi, 2003; Trisakti, Kartasmita & Kartika, 2009; Gao & Zhang, 2009b, 2009a; Balthazar, Vanacker & Lambin, 2012; Vanonckelen, Lhermitte & Van Rompaey, 2013; Li, Im & Beier, 2013; Gao *et al.*, 2016; Park *et al.*, 2017; Pimple *et al.*, 2017; Takaku & Tadono, 2017; Fan *et al.*, 2018; Phiri *et al.*, 2018; Umarhadi & Danoedoro, 2019; Zylshal, 2019). In this study, the 3-arc-second version of SRTM (Version 4) was used. We downloaded the data from the CIAT-CSI SRTM website (<http://srtm.csi.cgiar.org/>) (Jarvis *et al.*, 2008).

ALOS World 3D-30m (AW3D30) is a Japan Aerospace Exploration Agency (JAXA) project to provide DEM data. The project uses the ALOS PRISM panchromatic stereo sensor, which operated from 2006 to 2011. AW3D30 is a digital surface model (DSM) with a spatial resolution of 30 meters and was first released in March 2017 (Civco, 1989; Japan Aerospace Exploration Agency, 1997; Takaku *et al.*, 2016; Takaku & Tadono, 2017). We used the latest version (Version 3.1) released in April 2020. The data set was downloaded from JAXA's Earth Observation Research Center (EORC) (<https://www.eorc.jaxa.jp/ALOS/en/aw3d30/data/index.htm>) (Japan Aerospace Exploration Agency, 2020).

DEMNAS was developed and released by the Indonesian Geospatial Information Agency (BIG). It was built from several data sources, including IfSAR data (5 m resolution), TERRASAR-X (5 m resolution), and ALOS-PALSAR (11.25 m resolution), by adding/assimilating mass point data to stereo-plotting results. The spatial resolution of DEMNAS is 0.27 arc seconds, using EGM2008 vertical datum (BIG, 2018). The data was downloaded from the Indonesian Geospatial Agency website (<https://tanahair.indonesia.go.id/demnas>) (BIG, 2018). DEMNAS is produced by adding/assimilating mass point data into the DSM (IfSAR, TERASAR-X, or ALOS-PALSAR) using GMT surface with a tension of 0.32. Details of the assimilation process can be found in Hell and Jakobsson (2011). The official information on the DEMNAS website states that the data itself is considered as a digital terrain model (DTM). However, studies conducted by Julzarika and Harintaka (2019) argue that DEMNAS should be treated as a DSM rather than a DTM. In this study, we agree with this latter interpretation and treat DEMNAS as a DSM. The fact that SRTM and AW3D30 are also DSMs makes the comparison appropriate. **Table 1** summarizes the DEM data used in this study.

**Table 1.**

**The DEMs used in this study.**

No	DEM	Horizontal resolution	Vertical resolution	Vertical datum	Source
1	SRTM	30 m	16 m	EGM96	USGS
2	AW3D30	30 m	4.4 m	EGM96	JAXA
3	DEMNAS	8 m	5 m	EGM08	BIG

#### 3.2. SPOT-6/7

The SPOT-6/7 data used in this study is multispectral bands with 6-meter spatial resolution. Multispectral data was chosen based on the similarity of its resolution to that of DEMNAS (8 m). Furthermore, Standard Ortho (Astrium Services, 2013) products with less than 1 pixel (< 6 m) horizontal accuracy (CE90) were used instead of raw Level 1 (RSensor) data. The complete list of SPOT-6/7 data used is shown in **Table 2**. The data were cropped based on the AOI. The information needed as the input parameters for topographic correction were collected from SPOT-6/7 metadata, as shown in **Table 2**.

**Table 2.**

**SPOT-6/7 data specifications used in this study.**

AOI	Scene ID	Acquisition date	Acquisition time (GMT)	Viewing angle	Sun's azimuth	Sun's elevation
#1	SPOT6_201909140204066	Sept 14, 2019	02:04:06	21.16	76.26	60.96
#2	SPOT7_201710130156070	Oct 13, 2017	01:56:07	25.59	95.20	62.20

### 3.3. Methods

#### 3.3.1. Atmospheric correction

Several topographic correction methods require the satellite imagery to be atmospherically corrected (surface reflectance) (Richter, 1997; Riaño *et al.*, 2003; Vanonckelen *et al.*, 2014; Pimple *et al.*, 2017; Vázquez-Jiménez *et al.*, 2017; Phiri *et al.*, 2018). However, the use of top-of-atmosphere (TOA) reflectance is also not uncommon (Richter, Kellenberger & Kaufmann, 2009). In this study, the SPOT-6/7 imagery was corrected to surface reflectance value using the MODTRAN-4 algorithm (Adler-Golden *et al.*, 1999; Matthew *et al.*, 2000). Studies conducted by Fibriawati (2016) and Rotta *et al.* (2016) point out that MODTRAN-4 performs well for SPOT-6/7 imagery.

Each item of SPOT-6/7 data was converted to TOA reflectance by calculating the incoming solar irradiance. For SPOT-6/7 the TOA radiance is calculated as follows (Astrium Services, 2013):

$$\rho_b(p) = \frac{\mu \cdot L_b(p)}{E_0(b) \cdot \cos(\theta_s)} \quad (1)$$

$L_b(p)$  is the TOA radiance and is calculated as follows:

$$L_b(p) = \frac{DC(p)}{GAIN(b)} + BIAS(b) \quad (2)$$

where  $b$  is the respective band,  $DC(p)$  is the pixel value (digital number), and  $L_b(p)$  is the TOA radiance (in  $W \cdot [sr]^{-1} \cdot m^{-2} \cdot [\mu m]^{-1}$ ). GAIN and BIAS is the absolute radiometric calibration coefficient of SPOT-6/7.

The data is then converted to surface reflectance (SR) value using the MODTRAN-4 algorithm within the FLAASH® module in ENVI®. The program runs with an intuitive graphical user interface (GUI). The user needs to specify several input parameters to model the atmospheric conditions at the time of satellite image acquisition (ENVI, 2009). The input parameters used in this study are shown in **Table 3**.

**Table 3.**

**Input parameters in FLAASH®.**

FLAASH parameters	AOI 1	AOI 2
Sensor type	SPOT-6	SPOT-7
Sensor altitude	701.61 km	702.05 km
Ground elevation	0.8 km	0.3 km
Flight date (YYMMDD)	20190914	20171013
Flight time (HH:MM:SS) (GMT)	020406	015607
Atmospheric model	Tropical	Tropical
Aerosol model	Rural	Rural
Initial visibility	100 km	100 km
Zenith angle	29.12	27.89
Azimuth angle	209.1	178.7
Aerosol retrieval	2-band (K-T)	2-band (K-T)
KT upper channel	B3 (825 nm)	B3 (825 nm)
KT lower channel	B0 (485 nm)	B0 (485 nm)

#### 3.3.2. DEM processing

The SRTM data for AOI 2 contains several holes/gaps and so a gap-filling algorithm based on “GDAL fill no data” was applied (GDAL/OGR contributors, 2020). Each DEM was resampled into the same spatial resolution as SPOT-6/7 imagery (6 m). The purpose of resampling was to reduce the errors caused by overshooting the grid value beyond the edge of the pixels (Nichol & Hang, 2013). The resampling procedures were performed using a bilinear algorithm, chosen to reduce aliasing during the upscaling stage. The bilinear algorithm produces a smoothing effect on the resampled DEM (Parker, Kenyon & Troxel, 1983). The use of a smoothed DEM in topographic correction can increase its effectiveness (Riaño *et al.*, 2003; Richter, Kellenberger & Kaufmann, 2009; Goslee, 2012; Nichol & Hang, 2013). Slope and aspect were then derived for the DEMs to be used for further analysis.

Since each set of DEM data is originally delivered with different vertical datum, it then needs to be converted to a unified format. In this study, Earth Gravitational Model (EGM) 2008 (Kenyon & Factor, 2007) was used for all three DEMs.

### 3.3.3. Topographic correction

The first step in topographic correction using the Minnaert correction method is to calculate the local illumination of the test site. In this study, local illumination modeling was generated for each DEM and calculated as follows (Equation 3):

$$\cos i = \cos \theta_s \cos \theta_n(x, y) + \sin \theta_s \sin \theta_n \cos\{\phi_n(x, y) - \phi_s\} \quad (3)$$

where  $\cos i$  is the local solar illumination angle,  $\theta_n$  is the solar zenith angle,  $\theta_s$  is the terrain's slope,  $\phi_n$  is the solar azimuth, and  $\phi_s$  is the topographic azimuth. Meanwhile,  $x$  and  $y$  indicate the pixel's coordinates. The solar zenith and azimuth information were all taken from SPOT-6/7 metadata. The slope and topographic azimuth were derived from the DEM. The  $\cos i$  values range from -1 to 1 (Riaño *et al.*, 2003).

The Minnaert correction algorithm was chosen for this study. This method, proposed by Minnaert (1941), was originally developed to study the lunar surface; however, its performance in topographic correction makes it one of the most-cited non-Lambertian methods (Hantson & Chuvieco, 2011). Several studies have found that Minnaert correction is able to outperform other Lambertian-based topographic corrections (Colby, 1991; Law & Nichol, 2004; Gao *et al.*, 2016). The algorithm is based on a non-Lambertian assumption and introduces the Minnaert constant ( $k$ ) to the cosine method in the form of a bidirectional reflectance distribution function. The Minnaert correction can be written as follows (Riaño *et al.*, 2003):

$$\rho_H = \rho_T * \left( \frac{\cos \theta_n}{\cos i} \right)^k \quad (4)$$

where  $\rho_H$  denotes the reflectance of a horizontal surface, and  $\rho_T$  denotes the reflectance of an inclined surface. The  $k$  value for each band is calculated by linearization of Equation 4 into:

$$\ln(\rho_T) = \ln(\rho_H) + k \ln \left( \frac{\cos i}{\cos \theta_n} \right) \quad (5)$$

Letting  $\ln \left( \frac{\cos i}{\cos \theta_n} \right)$  be  $x$ ,  $\ln(\rho_T)$  be  $y$ , and  $\ln(\rho_H)$  be  $m$ , we end up with the linear function as follows:

$$y = kx + m \quad (6)$$

The  $k$  values can then be calculated using a linear regression function. The Minnaert constant depends on the land-cover type as well as the wavelength used (Gao *et al.*, 2016). The next step was to calculate the  $k$  constant for each image band on the same land-cover feature. Thus, a prior forest classification was employed on SPOT-6/7 imagery. Based on the landuse/land-cover sample points taken from the field survey conducted in 2020 at AOI 1 and in 2018 at AOI 2, a simple random forest (RF) classifier was employed on SPOT-6/7 imagery. The solar zenith and azimuth information is taken from SPOT-6/7 image metadata along with the derived slope and aspect data from the DEM. The next step was to calculate the  $k$  constant for each image band. Band-specific  $k$  value needs to be extracted from the same land-cover type; for this study we chose forest, as it covers a large portion of both AOIs.

After the forest class was acquired, 2000 sample points were randomly generated for each AOI. These sample points were then used to calculate the Minnaert constant ( $k$ ) for each SPOT-6/7 band and DEM used. The  $k$  value is based on the bidirectional reflectance distribution function and ranges from 0 to 1. The  $k$  value depends on the land-cover type as well as the image band. It is computed using a regression-fitting linear equation (Gao *et al.*, 2016). The  $k$  values are then fed into the Minnaert correction algorithm as shown in Equation 4.

### 3.3.4. Performance assessments

The pre-corrected and post-corrected images were compared to assess each DEM's performance. The topographically corrected images were evaluated both visually and statistically. Visual

assessment was employed to see whether there was any over- or under-correction. Meanwhile, for the statistical analysis, sample points were generated specifically for the sunlit and shaded slopes within the forested region. We opted to specifically investigate sunlit pixels and their direct opposite aspect pixels to understand better how topographic correction affects these pixels within SPOT-6/7 imagery. In this study, the sunlit samples were taken from all the pixels within the  $\pm 20^\circ$  range of each DEM's aspect from the sun's azimuth for the respective acquisition dates. The shaded region was taken from the exact opposite of the corresponding sunlit slope at  $180^\circ \pm 20^\circ$  range from the sun's azimuth. All these samples were forest pixels. We generated 200 random kernels for each AOI with a kernel size of  $9 \times 9$ . The sunlit and shaded pixels were all given 100 kernels each (**Table 4**).

**Table 4.****Number of sample points used for quantitative assessments.**

AOI	# Samples		Total
	Sunlit	Shade	
1	7647	7726	15,373
2	7766	7673	15,439

The pixel value of the pre-corrected and post-corrected images, as well as the local illumination value at the exact location, were extracted. Two methods of statistical evaluation were employed. First, the Pearson correlation ( $r$ ) between the local illumination and the pixel value was calculated (Holben & Justice, 1980; Justice, Wharton & Holben, 1981) and plotted using a scatterplot of density of forest land cover. The best performer should be able to reduce the pixel value's dependency on the topographic condition after correction. Second, the coefficient of variation (CV) was calculated. The CV is widely adopted to identify intra-class homogeneity (Gao & Zhang, 2009a). The difference between CV ( $CV_{diff}$ ) before and after correction was also calculated (Vanonckelen *et al.*, 2014; Pimple *et al.*, 2017; Zylshal, 2020). A successful topographic correction should also be able to reduce the CV. Finally, a matrix table comparing the three DEM sources was prepared and the best performers were ranked. The ranking was based on which DEM was able to reduce topographic dependency as well as CV without inducing over-/under-correction of visual appearance.

## 4. RESULTS AND DISCUSSIONS

### 4.1. Results

**Table 5** shows the local Minnaert constant ( $k$ ) used in this study for each band and DEM. The  $k$  values in AOI 2 are generally higher than AOI 1. The  $k$  values in AOI 1 range from 0.193 to 0.6254. The  $k$  value of the NIR band in AOI 1 is the highest value for each DEM, while the lowest  $k$  value appears in the blue band. These values were then fed into Equation 4 for each combination of bands and DEM for both AOIs.

**Table 5.****Results of Minnaert constant ( $k$ ) calculation.**

SPOT-6/7 band	AOI 1			AOI 2		
	SRTM	AW3D	DEMNAS	SRTM	AW3D	DEMNAS
B	0.4100	0.4108	0.1930	0.7801	0.8008	0.6505
G	0.4424	0.4712	0.3484	0.8327	0.7629	0.8103
R	0.4651	0.4961	0.3809	0.8323	0.7402	0.7943
NIR	0.5848	0.6254	0.5003	0.7256	0.6993	0.6913

#### 4.1.1. Visual evaluation

**Fig. 3** shows the effect of the Minnaert correction algorithm applied to both AOIs, presented in RGB color composite of red-NIR-blue. **Figs. 3A** and **3C** show the uncorrected SPOT-6/7 images for AOI 1 and AOI 2, respectively. **Figs. 3B** and **3D** show the corrected SPOT-6/7 images using AW3D30 over the corresponding AOIs. Both DEMNAS and SRTM yield very similar results when viewed at the overall zoom level of the AOIs.



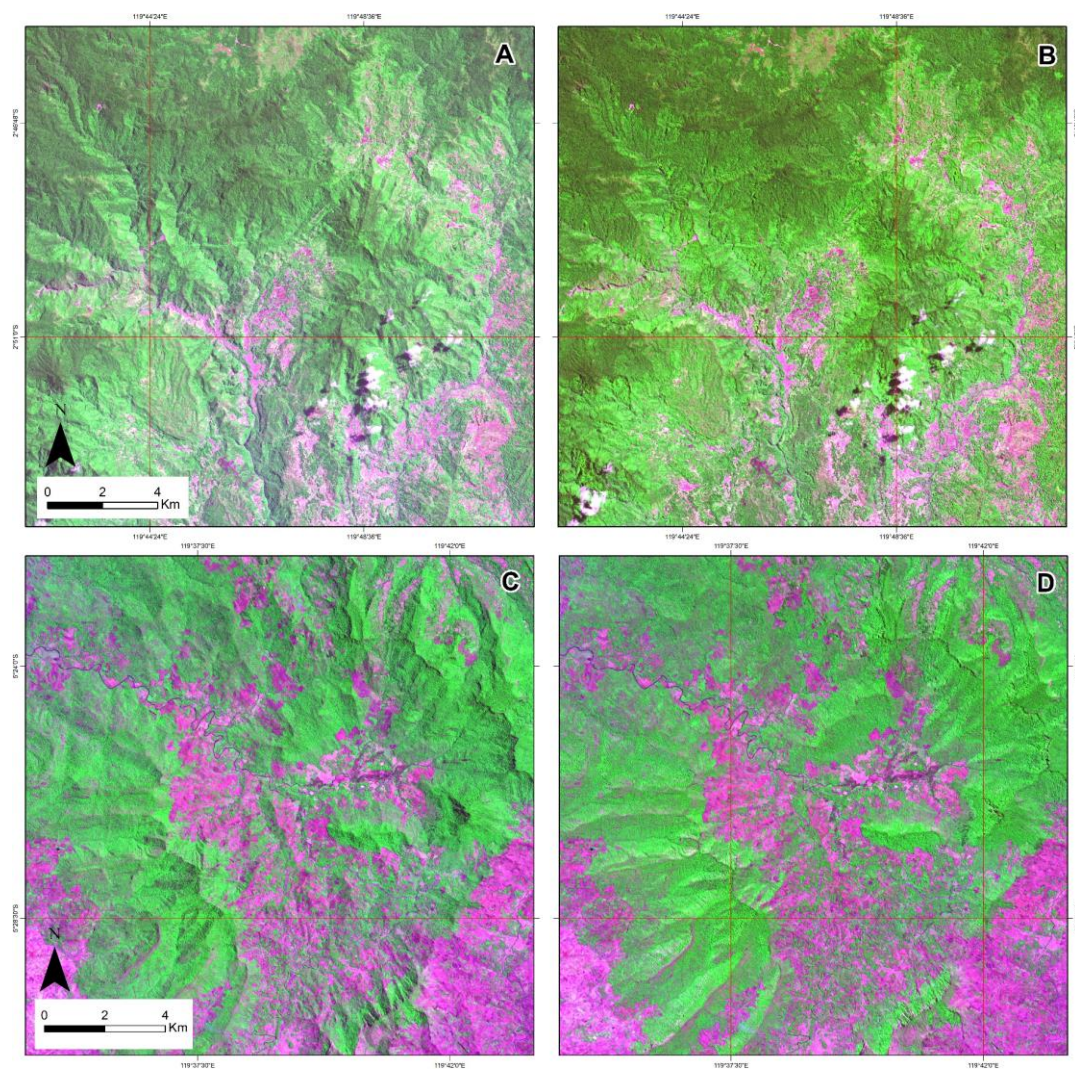


**Fig. 3.** Visual comparison of topographic correction over the entire AOI using AW3D30 (RGB composite of Red-NIR-Blue); (A) and (C).

The different visual performances, only visible over some areas and with added zoom level, are as shown in **Fig. 4**. The more obvious visual comparisons of all three DEMs, as well as corresponding topographic correction results, are shown in **Fig. 4**. Compared to the pre-corrected images (**Figs. 4A** and **4I**), the use of Minnaert correction on SPOT-6/7 data is visually successful for both AOIs. The different facing slopes on the same forest land cover appear to be in the same contrast and brightness (**Figs. 4B, 4C, 4D, 4F, 4G, and 4H**). A closer inspection (yellow circle) shows that under-correction occurs on SRTM for both AOIs, as shown in **Figs. 4B, 4F, 4J, and 4N**. AW3D30 and DEMNAS produce a very similar result on AOI 1, as shown in **Figs. 4C** and **4D**. However, AW3D30 has a slight advantage in performance, as shown in the yellow circle in **Fig. 4G** compared to the slightly under-corrected DEMNAS version (**Fig. 4H**). For AOI 2, AW3D30 and DEMNAS perform better visually (**Fig. 4J** and **Fig. 4K**, respectively) than SRTM (**Fig. 4J**). While similar overall, DEMNAS shows over-correction in several areas, mostly located on hill ridges, as indicated by the yellow circle in **Fig. 4P**. AW3D30 also suffered slight over-correction over the same region (**Fig. 4O**), albeit not as high as that of DEMNAS. Visually, AW3D30 performed the best, with DEMNAS a close second, and SRTM performing the least successfully.



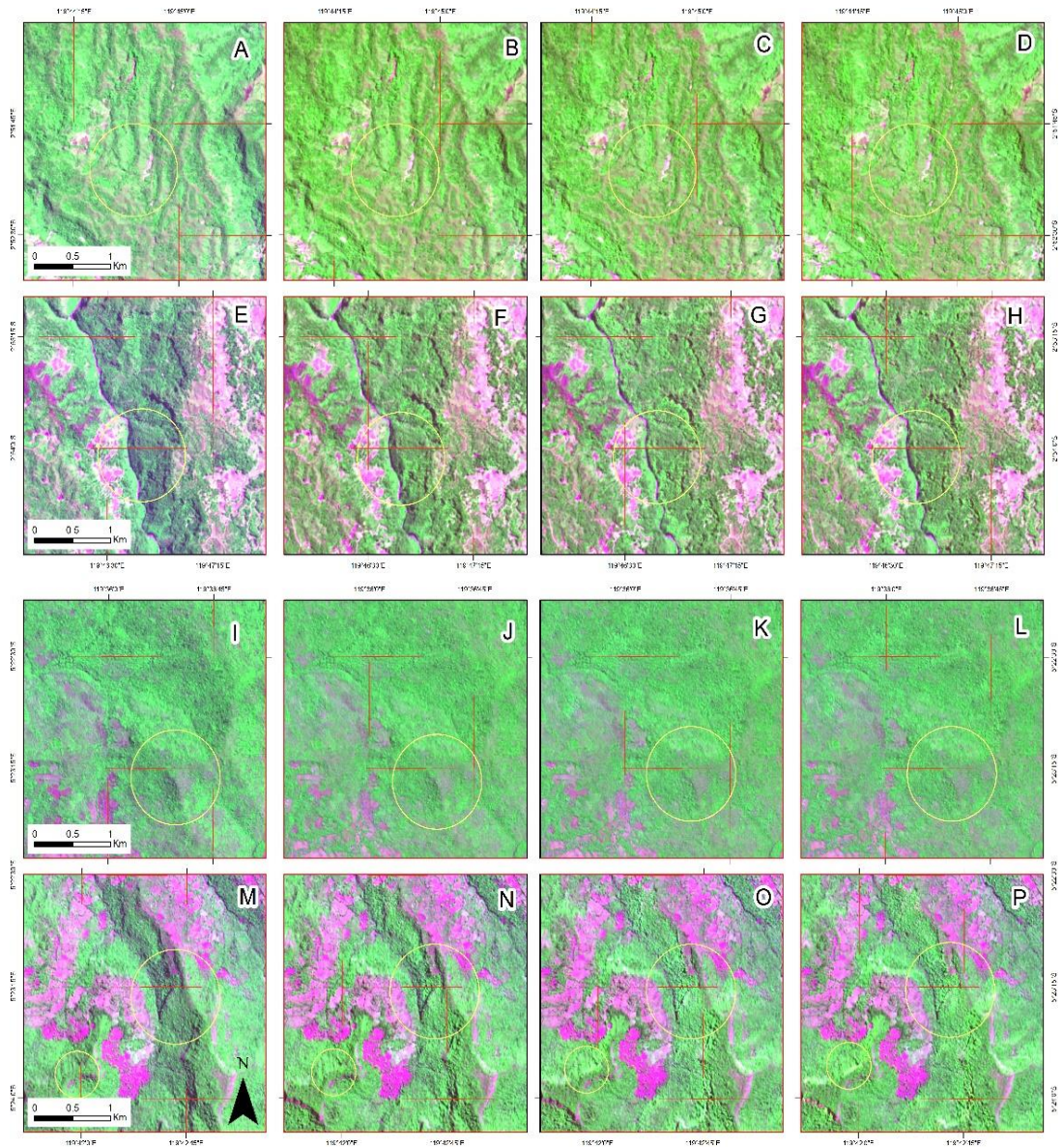


**Fig. 4.** Visual comparison of topographic correction shown in “natural-color” RGB composite of Red–NIR–Blue over several subset regions of the test sites: pre-corrected surface reflectance SPOT-6/7 on AOI 1 (A and E); topographically corrected AOI 1 using SRTM (B and F), AW3D30 (C and G), and DEMNAS (D and H). Pre-corrected surface reflectance of SPOT-6/7 on AOI 2 (I and M). Topographically corrected AOI2 using SRTM (J and N), AW3D30 (K and O), and DEMNAS (L and P). The yellow circle emphasizes the different performance of each data set.

#### 4.1.1. Quantitative evaluation

**Fig. 5** confirms the effect of performing topographic correction on the SPOT-6/7 data. The trend line’s gradient has been reduced after the topographic correction. The flat trend line means that the terrain’s influence on the image’s reflectance value has been reduced. The sun-facing slopes and the slopes facing away from the sun have similar reflectance values. The complete list of how the trend-line gradients ( $m$ ) and  $r$  change for all data sets in each AOI are shown in **Table 6**.

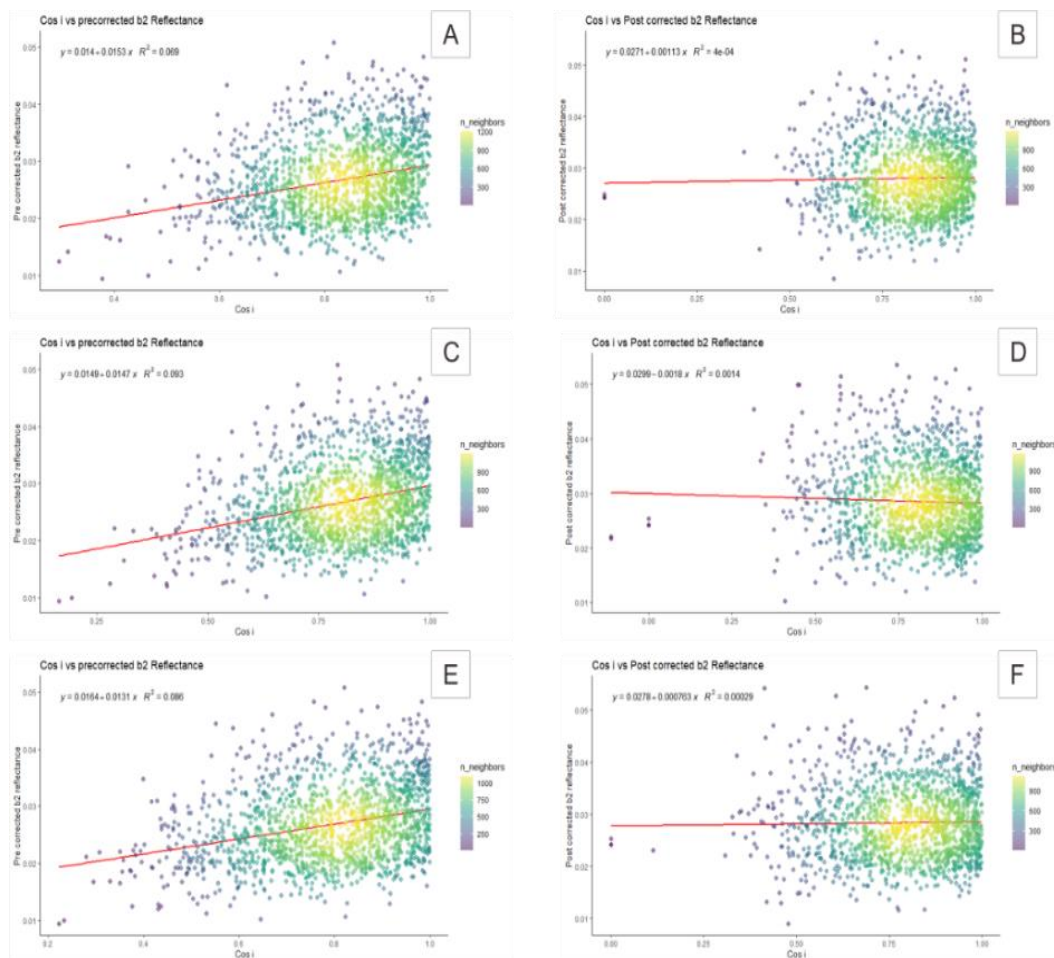


**Fig. 5.** Scatterplot density between *cos i* and surface reflectance for AOI 1 before and after topographic correction applied to SPOT-6/7 green band: (A) Pre-corrected using SRTM; (B) post-corrected using SRTM; (C) pre-corrected using AW3D30; (D) post-corrected using AW3D30; (E) pre-corrected using DEMNAS; (F) post-corrected using DEMNAS.

**Table 6.**

**Trend-line gradient (*m*) and Pearson correlation (*r*) values before and after correction.**

AOI	Band	<i>m</i> SRTM		<i>m</i> AW3D30		<i>m</i> DEMNAS		<i>r</i> SRTM		<i>r</i> AW3D30		<i>r</i> DEMNAS	
		Pre	Post	Pre	Post	Pre	Post	Pre	Post	Pre	Post	Pre	Post
		1	B	0.0016	0.0012	0.0016	0.0008	0.0018	0.0013	0.4520	0.2990	0.3820	0.1650
1	G	0.0014	0.0010	0.0017	0.0008	0.0017	0.0012	0.6200	0.4170	0.6160	0.2830	0.6150	0.3870
1	R	0.0020	0.0014	0.0025	0.0011	0.0026	0.0016	0.6590	0.4020	0.6710	0.2530	0.6670	0.3690
1	NIR	0.0002	0.0001	0.0002	0.0000	0.0002	0.0001	0.6570	0.2950	0.6930	0.1060	0.6850	0.2560
2	B	0.0017	0.0007	0.0021	-0.0003	0.0022	0.0002	0.4602	0.1862	0.4930	-0.0788	0.5027	0.0415
2	G	0.0011	0.0007	0.0014	-0.0003	0.0014	-0.0004	0.6388	0.3036	0.6734	-0.1111	0.6803	-0.1836
2	R	0.0009	0.0004	0.0011	-0.0002	0.0011	-0.0003	0.4721	0.1867	0.4922	-0.0788	0.4951	-0.1308
2	NIR	0.0002	0.0001	0.0002	0.0000	0.0002	0.0000	0.0002	0.0001	0.7770	-0.0600	0.7852	-0.0589

The SR of pre-corrected images shows a statistically significant correlation to local illumination at 95% confidence level. The Pearson correlation varied with each DEM and SPOT-6/7 band. Prior to correction, the  $r$  value varied from 0.0002 to 0.66 for SRTM, 0.38 to 0.78 for AW3D30, and 0.41 to 0.79 for DEMNAS. After correction, all DEMs were able to reduce  $m$  as well as  $r$ . AW3D30 produced the highest reduction of the correlation on five bands: blue on both AOIs, and green, red, and NIR on AOI 1. DEMNAS performed second best with the three highest CV reductions on green, red, and NIR, all in AOI 2. It is worth noting that in AOI 2, both AW3D30 and DEMNAS produced negative  $r$  values, specifically for green and red bands. The negative  $r$  value is the quantitative representation of the over-correction shown in **Figs. 4O** and **4P**.

The under-correction produced by SRTM is confirmed by the total reduction of  $r$  in **Table 6**. Apart from the blue band for AOI 1, SRTM consistently produced the least reduction in  $r$  for all bands for both AOIs. All DEMs are able to produce higher CV reduction on the NIR band for both AOIs. This is easily explained by the fact that the sample points used were taken on a highly vegetated area (forest land cover) where the spectral value in NIR is typically higher than the visible bands. With these results, we then moved on to calculate the intra-class spectral homogeneity using CV.

**Table 7** shows the CV for each band before and after topographic correction, as well as the difference between them. The best performer is that which produces the greatest reduction in CV (Riaño *et al.*, 2003; Richter, Kellenberger & Kaufmann, 2009). AW3D30 produces the greatest CV reduction on the NIR band with a total of 14.23 for both AOIs. As with the correlation value, the value of CV also varied with wavelength (band). SRTM produced the highest CV reduction on four occasions: blue on AOI 1 and AOI 2, and green and red on AOI 2. AW3D30 performed the second-best CV reduction, with three bands having the most reduced CV (green, red, and NIR on AOI 1). DEMNAS came out last with the least number of bands having reduced CV.

**Table 7.**

**CV for each band before and after topographic correction. Bold CV value marks the best performer.**

AOI	Band	Original CV	CV			CV <sub>dif</sub>		
			AW3D30	DEMNAS	SRTM	AW3D30	DEMNAS	SRTM
1	B	194.7179	122.7256	121.662	121.3415	71.99	73.06	<b>73.38</b>
	G	37.01004	31.92108	32.50429	32.61597	<b>5.09</b>	4.51	4.39
	R	31.31638	25.69942	26.22724	26.68509	<b>5.62</b>	5.09	4.63
	NIR	30.2518	21.3648	21.72446	22.96099	<b>8.89</b>	8.53	7.29
2	B	41.25368	40.48688	39.43436	38.60342	0.77	1.82	<b>2.65</b>
	G	30.25273	23.63064	24.34279	23.41615	6.62	5.91	<b>6.84</b>
	R	40.66021	38.52378	39.65421	36.84552	2.14	1.01	<b>3.81</b>
	NIR	24.46119	19.11675	19.0159	19.67073	5.34	<b>5.45</b>	4.79

## 5. DISCUSSION

Based on visual appearance, the reduction of  $cos i$  correlation with surface reflectance, and CV reduction, it is clear that AW3D30 is best suited to being used as the DEM for topographic correction on SPOT-6/7 data (**Table 8**), provided that the Minnaert algorithm is used. This study is the first proof of the suitability of AW3D30 as a DEM source for correcting topographic effects on SPOT-6/7 imagery. Our results are in agreement with results obtained by other authors when comparing different DEM data for topographic correction (Hantson & Chuvieco, 2011; Pimple *et al.*, 2017). The coarser spatial resolution of AW3D30 compared to SPOT-6/7 did not make it inferior to other DEMs with higher spatial resolution (DEMNAS).

Table 8.

Comparison matrix of all DEMs ranked based on the performance assessment used.

DEM	Rankings of performance assessments		
	Visual evaluation	Number of bands with the most reduced $r$	Number of bands with the most reduced CV
AW3D30	1	1	2
DEMNAS	2	2	3
SRTM	3	3	1

Our results also confirm other authors' findings that there is no single source of data or algorithm that is superior in every case (Richter, Kellenberger & Kaufmann, 2009; Ghasemi, Mohammadzadeh & Sahebi, 2011). A similar study conducted in the same area by Zylshal (2019) shows that AW3D30 is superior to DEMNAS, albeit for different EO satellite images. Our study confirms the consensus that the best method varies with different combinations of satellite imagery, study area size (Richter, Kellenberger & Kaufmann, 2009), existing land cover (Gao & Zhang, 2009a), and correction algorithm (Pimple *et al.*, 2017).

Considering the above, our findings are also constrained by the use of the Minnaert algorithm. While it has been shown to have performed well in our study as well as in several other studies (Colby, 1991; Law & Nichol, 2004; Gao *et al.*, 2016), the fact that our test sites are located in a forested mountainous region opens up the possibility of using a different algorithm. Several methods for Minnaert modification have been proposed, including pixel-based Minnaert (PMB) based on slope stratification (Lu *et al.*, 2008), modified Minnaert with IL stratification (Ekstrand, 1996), and SCS + Minnaert (Reeder, 2002). While these approaches may have the potential to perform better than the traditional Minnaert algorithm, algorithm comparison is outside this paper's scope. Another limitation is the fact that the DEMNAS data used in our study is only available for the Indonesian region. Hence, the exact reproducibility of our study in another regions of the world is limited. Crucially, AW3D30 is available worldwide for free, strengthening our confidence in the reproducibility of our results. It is worth noting that our study employed AW3D30 version 3.1 and in several regions, due to cloud and snow cover, AW3D30 still has voids (Takaku & Tadono, 2017). Version 3.2 has since been released with additional tiles to fill these voids. Therefore, we recommend using the newest AW3D30 data available for such regions.

Our study also found that the total area of corrected imagery was also reduced, as reported by Hantson and Chuvieco (2011). The main cause was the fact that local illumination was calculated using a kernel window of  $3 \times 3$  of the surrounding pixels, causing the edges of the produced images to be practically reduced by 1 pixel. While the best way to mitigate area reduction is by using a DEM with one-third of the pixel size of the image, as suggested by Hantson and Chuvieco (2011), such DEM is unfortunately still not available for our study area. Our recommendation, instead, is to use a slightly wider initial test site than the original AOI and to crop the corrected image at a later stage. While our solution might work with a definitive AOI boundary such as a rectangle, watershed, or administrative boundary, problems might occur when the correction is conducted on a scene-by-scene basis. While AW3D30 has proven to be the best performer, DEMNAS and SRTM also produce adequate results. Since both of these data sources have shown better performance using other algorithms, SRTM's under-correction issue found in this study could be mitigated by using algorithms other than the Minnaert. Alternatively, the over-correction produced by DEMNAS could be mitigated by performing a smoothing filter prior to calculating the  $\cos i$ , as recommended by Riaño *et al.* (2003) and Goslee (2012). The newly released TanDEM-X 90m DEM (TDX90), as well as Copernicus 90 and 30 m DEM, will also be interesting to investigate, given their comparable horizontal and vertical accuracy to AW3D30 (Wessel, 2016). A previous study found that the SCS model is better for use in forest regions (Gu & Gillespie, 1998), while others have argued that the pixel-based Minnaert algorithm is more suitable (Ghasemi, Mohammadzadeh & Sahebi, 2011). It is, however, worth noting that these previous studies were all conducted using coarser satellite data and DEM sources. It would be interesting to investigate whether the use of other algorithms would still produce the same results as ours.



## 6. CONCLUSIONS

Topographic correction using the Minnaert algorithm was successfully performed on SPOT-6/7 multispectral data. The performance of three different DEMs (DEMNAS, AW3D30, and SRTM) was also successfully assessed and compared. Topographic correction was performed on two different test sites. Based on our performance assessment, both visual and statistical, AW3D30 outperformed the other DEMs. Visual assessment showed that AW3D30 was able to reduce the radiometric difference between sun-facing slopes and slopes facing away from the sun with no over- or under-correction visible. In statistical evaluation, AW3D30 was able to produce the highest reduction of a pixel value's dependency to its corresponding topography in the SPOT-6/7 images tested.

We can conclude that AW3D30 is the best option for correction of topographic distortion on SPOT-6/7 imagery for the Indonesian region. Tweaks and modifications, however, are necessary to resolve the under-correction present when using SRTM or the over-correction when using DEMNAS on SPOT-6/7 imagery. Considering the similar spatial resolution, it is highly advisable to further investigate the performance of DEMNAS using other algorithms.

## ACKNOWLEDGMENTS

We would like to thank Dr. Ari Widyanti of Institut Teknologi Bandung and Prof. Iskhaq Iskandar of Universitas Sriwijaya for their constructive inputs during the early draft of this paper. The SPOT-6/7 data were provided by LAPAN Remote Sensing Technology and Data Center.

## REFERENCES

- Adler-Golden, S. M. *et al.* (1999) 'Atmospheric correction for short-wave spectral imagery based on MODTRAN4', in *Proceedings of SPIE - The International Society for Optical Engineering*. Denver, USA: Society of Photo-Optical Instrumentation Engineers, Bellingham, WA, United States, pp. 61–69. Available at: <https://www.scopus.com/record/display.uri?eid=2-s2.0-0033348265&origin=inward>.
- Astrium Services (2013) 'SPOT 6 & SPOT 7 imagery user guide', *Astrium Services*, (July), p. 120.
- Balthazar, V., Vanacker, V. and Lambin, E. F. (2012) *Evaluation and parameterization of ATCOR3 topographic correction method for forest cover mapping in mountain areas*, *International Journal of Applied Earth Observation and Geoinformation*. Elsevier B.V. doi: 10.1016/j.jag.2012.03.010.
- BIG (2018) *DEMNAS - Seamless Digital Elevation Model (DEM) dan Batimetri Nasional*. Available at: <https://tanahair.indonesia.go.id/demnas>.
- Chavez Jr., P. S. (1996) 'Image-Based Atmospheric Corrections - Revisited and Improved', *Photogrammetric Engineering & Remote Sensing*, 62(10), pp. 1025–1036. Available at: <https://pdfs.semanticscholar.org/45f1/2625ce130261c7d360d50e09c635355ca919.pdf>.
- Chen, R. *et al.* (2020) 'Evaluation and normalization of topographic effects on vegetation indices', *Remote Sensing*, 12(14). doi: 10.3390/rs12142290.
- Civco, D. L. (1989) 'Topographic Normalization of Landsat Thematic Mapper Digital Imagery', *Photogrammetric Engineering and Remote Sensing*, 55(9), pp. 1303–1309. Available at: [https://www.asprs.org/wp-content/uploads/pers/1989journal/sep/1989\\_sep\\_1303-1309.pdf](https://www.asprs.org/wp-content/uploads/pers/1989journal/sep/1989_sep_1303-1309.pdf).
- Colby, J. D. (1991) 'Topographic normalization in rugged terrain', *Photogrammetric Engineering & Remote Sensing*, 57(5), pp. 531–537.
- Ekstrand, S. (1996) 'Landsat TM-based forest damage assessment: Correction for topographic effects', *Photogrammetric Engineering and Remote Sensing*, 62(2), pp. 151–161.
- ENVI (2009) 'ENVI Atmospheric Correction Module: QUAC and FLAASH user's guide', *Module Version*, p. 44. Available at: <http://scholar.google.com/scholar?hl=en&btnG=Search&q=intitle:ENVI+Atmospheric+Correction+Module:+QUAC+and+FLAASH+user's+guide#0>.
- Fan, W. *et al.* (2018) 'Topographic correction of forest image data based on the canopy reflectance model for sloping terrains in multiple forward mode', *Remote Sensing*, 10(5). doi: 10.3390/rs10050717.

- Fibriawati, L. (2016) 'Koreksi Atmosfer Citra SPOT-6 Menggunakan Metode MODTRAN4', in *Seminar Nasional Penginderaan Jauh 2016*. Depok, Jawa Barat: LAPAN, pp. 98–104. Available at: [http://repository.lapan.go.id/index.php?p=show\\_detail&id=5362](http://repository.lapan.go.id/index.php?p=show_detail&id=5362).
- Gao, M. *et al.* (2016) 'An improved topographic correction model based on Minnaert', *GIScience and Remote Sensing*, 53(2), pp. 247–264. doi: 10.1080/15481603.2015.1118976.
- Gao, Y. and Zhang, W. (2009a) 'A simple empirical topographic correction method for ETM + imagery', *International Journal of Remote Sensing*, 30(9), pp. 2259–2275. doi: 10.1080/01431160802549336.
- Gao, Y. and Zhang, W. (2009b) 'LULC classification and topographic correction of Landsat-7 ETM+ Imagery in the Yangjia river Watershed: The influence of DEM resolution', *Sensors*, 9(3), pp. 1980–1995. doi: 10.3390/s90301980.
- GDAL/OGR contributors (2020) 'GDAL/OGR Geospatial Data Abstraction software Library'. Available at: <https://gdal.org>.
- Ghasemi, N., Mohammadzadeh, A. and Sahebi, M. R. (2011) 'Assessment of different topographic correction methods in ALOS AVNIR-2 data over a forest area', *International Journal of Digital Earth*, 6(5), pp. 504–520. doi: 10.1080/17538947.2011.625049.
- Goslee, S. C. (2012) 'Topographic corrections of satellite data for regional monitoring', *Photogrammetric Engineering and Remote Sensing*, 78(9), pp. 973–981. doi: 10.14358/PERS.78.9.973.
- Goyal, S. K., Seyfried, M. S. and O'Neill, P. E. (1998) 'Effect of digital elevation model resolution on topographic correction of airborne SAR', *International Journal of Remote Sensing*, 19(16), pp. 3075–3096. doi: 10.1080/014311698214190.
- Gu, D. and Gillespie, A. (1998) 'Topographic normalization of Landsat TM images of forest based on subpixel Sun-canopy-sensor geometry', *Remote Sensing of Environment*, 64(2), pp. 166–175. doi: 10.1016/S0034-4257(97)00177-6.
- Hantson, S. and Chuvieco, E. (2011) 'Evaluation of different topographic correction methods for landsat imagery', *International Journal of Applied Earth Observation and Geoinformation*, 13(5), pp. 691–700. doi: 10.1016/j.jag.2011.05.001.
- Hell, B. and Jakobsson, M. (2011) 'Gridding heterogeneous bathymetric data sets with stacked continuous curvature splines in tension', *Marine Geophysical Research*, 32(4), pp. 493–501. doi: 10.1007/s11001-011-9141-1.
- Hlatshwayo, S. T. *et al.* (2019) 'Mapping forest aboveground biomass in the reforested Buffelsdraai landfill site using texture combinations computed from SPOT-6 pan-sharpened imagery', *International Journal of Applied Earth Observation and Geoinformation*, 74(July 2018), pp. 65–77. doi: 10.1016/j.jag.2018.09.005.
- Holben, B. N. and Justice, C. O. (1980) 'The Topographic Effect on Spectral Response from Nadir-Pointing Sensors', *Photogrammetric Engineering & Remote Sensing*, 46, pp. 1191–1200. Available at: [https://www.asprs.org/wp-content/uploads/pers/1980journal/sep/1980\\_sep\\_1191-1200.pdf](https://www.asprs.org/wp-content/uploads/pers/1980journal/sep/1980_sep_1191-1200.pdf).
- Japan Aerospace Exploration Agency, E. O. R. C. (1997) 'ALOS Global Digital Surface Model "ALOS World 3D - 30m (AW3D30)" - Product Description', *Japan Aerospace Exploration Agency*. Available at: <https://www.eorc.jaxa.jp/ALOS/en/aw3d30/>.
- Japan Aerospace Exploration Agency (2020) *ALOS Global Digital Surface Model 'ALOS World 3D - 30m (AW3D30)'*. Available at: <https://www.eorc.jaxa.jp/ALOS/en/aw3d30/>.
- Jarvis, A. *et al.* (2008) *Hole-filled seamless SRTM data V4*, *International Centre for Tropical Agriculture (CIAT)*. Available at: <http://srtm.csi.cgiar.org>. (Accessed: 10 July 2020).
- Julzarika, A. and Durdjani (2019) 'DEM classifications: opportunities and potential of its applications', *J. Degrad. Min. Land Manage*, 6(4), pp. 1897–1905. doi: 10.15243/jdmlm.2019.064.1897.
- Julzarika, A. and Harintaka (2019) 'Indonesian DEMNAS: DSM or DTM?', in *AGERS 2019 - 2nd IEEE Asia-Pacific Conference on Geoscience, Electronics and Remote Sensing Technology*. Jakarta, Indonesia, Indonesia: IEEE, pp. 31–36. doi: 10.1109/AGERS48446.2019.9034351.
- Justice, C. O., Wharton, S. W. and Holben, B. N. (1981) 'Application of digital terrain data to quantify and reduce the topographic effect on landsat data', *International Journal of Remote Sensing*, 2(3), pp. 213–230. doi: 10.1080/01431168108948358.
- Kawata, Y., Ueno, S. and Kusaka, T. (1988) 'Radiometric correction for atmospheric and topographic effects on landsat mss images', *International Journal of Remote Sensing*, 9(4), pp. 1–2. doi: 10.1080/01431168808954889.

- Kenyon, S. and Factor, J. (2007) 'Towards The Next Earth Gravitational Model', in *The 77th Annual Meeting of Society of Exploration Geophysicist*. San Antonio, Texas, USA, p. 2. Available at: [https://earth-info.nga.mil/GandG/wgs84/gravitymod/new\\_egm/EGM08\\_papers/EGM-2007-final.pdf](https://earth-info.nga.mil/GandG/wgs84/gravitymod/new_egm/EGM08_papers/EGM-2007-final.pdf).
- Law, K. H. and Nichol, J. (2004) 'Topographic correction for differential illumination effects on ikonos satellite imagery', *XXth ISPRS Congress, XXXV Part*, pp. 641–646. Available at: <http://www.cartesia.org/geodoc/isprs2004/comm3/papers/347.pdf>.
- Leprieux, C. E., Durand, J. M. and Peyron, J. L. (1988) 'Influence of topography on forest reflectance using Landsat Thematic Mapper and digital terrain data', *Photogrammetric Engineering and Remote Sensing*, 54(4), pp. 491–496.
- Li, M., Im, J. and Beier, C. (2013) 'Machine learning approaches for forest classification and change analysis using multi-temporal Landsat TM images over Huntington Wildlife Forest', *GIScience and Remote Sensing*, 50(4), pp. 361–384. doi: 10.1080/15481603.2013.819161.
- Li, W. *et al.* (2015) 'Geostatistical modeling using LiDAR-derived prior knowledge with SPOT-6 data to estimate temperate forest canopy cover and above-ground biomass via stratified random sampling', *International Journal of Applied Earth Observation and Geoinformation*, 41, pp. 88–98. doi: 10.1016/j.jag.2015.04.020.
- Lu, D. *et al.* (2008) 'Pixel-based Minnaert correction method for reducing topographic effects on a landsat 7 ETM+ image', *Photogrammetric Engineering and Remote Sensing*, 74(11), pp. 1343–1350. doi: 10.14358/pers.74.11.1343.
- Matthew, M. W. *et al.* (2000) 'Status of atmospheric correction using a MODTRAN4-based algorithm', *Algorithms for Multispectral, Hyperspectral, and Ultraspectral Imagery VI*, 4049, p. 199. doi: 10.1117/12.410341.
- Minnaert, M. (1941) 'The reciprocity principle in lunar photometry', *The Astrophysical Journal*, 93(2), pp. 403–410. doi: 10.1086/144279.
- Motlagh, M. G. *et al.* (2018) 'Estimating and mapping forest biomass using regression models and Spot-6 images (case study: Hyrcanian forests of north of Iran)', *Environmental Monitoring and Assessment*, 190(6). doi: 10.1007/s10661-018-6725-0.
- Nguyen, T. D. and Kappas, M. (2020) 'Estimating the aboveground biomass of an evergreen broadleaf forest in Xuan Lien Nature Reserve, Thanh Hoa, Vietnam, using SPOT-6 data and the random forest algorithm', *International Journal of Forestry Research*, 2020. doi: 10.1155/2020/4216160.
- Nichol, J. and Hang, L. K. (2013) 'The Influence of DEM Accuracy on Topographic Correction of Ikonos Satellite Images', *Photogrammetric Engineering & Remote Sensing*, 74(1), pp. 47–53. doi: 10.14358/pers.74.1.47.
- Nkwunonwo, U. C., Whitworth, M. and Baily, B. (2020) 'A review of the current status of flood modelling for urban flood risk management in the developing countries', *Scientific African*, 7, p. e00269. doi: 10.1016/j.sciaf.2020.e00269.
- Nonin, P. *et al.* (2013) *3D Capabilities of Spot 6*. Available at: [http://www.intelligence-airbusds.com/files/pmedia/public/r28533\\_9\\_icc2013\\_3d\\_capabilities\\_of\\_spot\\_6.pdf](http://www.intelligence-airbusds.com/files/pmedia/public/r28533_9_icc2013_3d_capabilities_of_spot_6.pdf).
- Park, S. H. *et al.* (2017) 'A quantitative method to evaluate the performance of topographic correction models used to improve land cover identification', *Advances in Space Research*, 60(7), pp. 1488–1503. doi: 10.1016/j.asr.2017.06.054.
- Parker, J. a, Kenyon, R. V and Troxel, D. E. (1983) 'Comparison of interpolation methods for image resampling', *IEEE Transactions on Medical Imaging*, 2(1), pp. 31–39. doi: 10.1109/42.7784.
- Phiri, D. *et al.* (2018) 'Effects of pre-processing methods on Landsat OLI-8 land cover classification using OBIA and random forests classifier', *International Journal of Applied Earth Observation and Geoinformation*, 73(April), pp. 170–178. doi: 10.1016/j.jag.2018.06.014.
- Pimple, U. *et al.* (2017) 'Topographic correction of Landsat TM-5 and Landsat OLI-8 imagery to improve the performance of forest classification in the mountainous terrain of Northeast Thailand', *Sustainability (Switzerland)*, 9(2), pp. 1–26. doi: 10.3390/su9020258.
- Rani, M. S. *et al.* (2017) 'The Effect of Topographic Correction on SPOT6 Land Cover Classification in Water Catchment Areas in Bandung Basin, Indonesia', *GISRUK 2017 Proceedings*. Manchester: Geographical Information Science Research UK. Available at: <http://eprints.whiterose.ac.uk/115753/>.
- Reeder, D. H. (2002) *Topographic correction of satellite images: Theory and application*. Dartmouth College.

- Riaño, D. *et al.* (2003) 'Assessment of different topographic corrections in landsat-TM data for mapping vegetation types (2003)', *IEEE Transactions on Geoscience and Remote Sensing*, 41(5 PART 1), pp. 1056–1061. doi: 10.1109/TGRS.2003.811693.
- Richter, R. (1997) 'Correction of atmospheric and topographic effects for high spatial resolution satellite imagery', *International Journal of Remote Sensing*, 18(5), pp. 1099–1111. doi: 10.1080/014311697218593.
- Richter, R., Kellenberger, T. and Kaufmann, H. (2009) 'Comparison of topographic correction methods', *Remote Sensing*, 1(3), pp. 184–196. doi: 10.3390/rs1030184.
- Rotta, L. H. S. *et al.* (2016) 'Atmospheric correction assessment of SPOT-6 image and its influence on models to estimate water column transparency in tropical reservoir', *Remote Sensing Applications: Society and Environment*, 4, pp. 158–166. doi: 10.1016/j.rsase.2016.09.001.
- Shepherd, J. D. and Dymond, J. R. (2003) 'Correcting satellite imagery for the variance of reflectance and illumination with topography', *International Journal of Remote Sensing*, 24(17), pp. 3503–3514. doi: 10.1080/01431160210154029.
- Takaku, J. *et al.* (2016) 'Validation of "Aw3D" Global Dsm Generated From Alos Prism', *ISPRS Annals of Photogrammetry, Remote Sensing and Spatial Information Sciences*, III-4(July), pp. 25–31. doi: 10.5194/isprsannals-III-4-25-2016.
- Takaku, J. and Tadono, T. (2017) 'Quality updates of "AW3D" global DSM generated from ALOS PRISM', *2017 IEEE International Geoscience and Remote Sensing Symposium (IGARSS)*, pp. 5666–5669. doi: 10.1109/IGARSS.2017.8128293.
- Trisakti, B., Kartasmita, M. and Kartika, T. (2009) 'Kajian Koreksi Terrain Pada Citra Landsat Thematic Mapper ( Tm )', *Jurnal Penginderaan Jauh*, 6, pp. 1–10.
- Umarhadi, D. A. and Danoedoro, P. (2019) 'Correcting topographic effect on Landsat-8 images: an evaluation of using different DEMs in Indonesia', (November 2019), p. 41. doi: 10.1117/12.2549109.
- Vanonckelen, S. *et al.* (2014) 'Performance of atmospheric and topographic correction methods on Landsat imagery in mountain areas', *International Journal of Remote Sensing*, 35(13), pp. 4952–4972. doi: 10.1080/01431161.2014.933280.
- Vanonckelen, S., Lhermitte, S. and Van Rompaey, A. (2013) 'The effect of atmospheric and topographic correction methods on land cover classification accuracy', *International Journal of Applied Earth Observation and Geoinformation*, 24(1), pp. 9–21. doi: 10.1016/j.jag.2013.02.003.
- Vázquez-Jiménez, R. *et al.* (2017) 'Topographic Correction to Landsat Imagery through Slope Classification by Applying the SCS + C Method in Mountainous Forest Areas', *ISPRS International Journal of Geo-Information*, 6(9), p. 287. doi: 10.3390/ijgi6090287.
- Vincini, M. and Frazzi, E. (2003) 'Multitemporal Evaluation of Topographic Normalization Methods on Deciduous Forest TM Data', *IEEE Transactions on Geoscience and Remote Sensing*, 41(11), pp. 2586–2590.
- Wessel, B. (2016) *TanDEM-X Ground Segment DEM Products Specification Document, Public Document TD-GS-PS-0021*. Available at: <https://tandemx-science.dlr.de/> (Accessed: 1 October 2020).
- Wu, J. *et al.* (2008) 'A comparison of illumination geometry-based methods for topographic correction of QuickBird images of an undulant area', *ISPRS Journal of Photogrammetry and Remote Sensing*, 63(2), pp. 223–236. doi: 10.1016/j.isprsjprs.2007.08.004.
- Wu, Q., Jin, Y. and Fan, H. (2016) 'Evaluating and comparing performances of topographic correction methods based on multi-source DEMs and Landsat-8 OLI data', *International Journal of Remote Sensing*, 37(19), pp. 4712–4730. doi: 10.1080/01431161.2016.1222101.
- Zylshal, Z. (2019) 'Performance evaluation of different DEMs for topographic correction on LAPAN-A3: preliminary results', in *Sixth Geoinformation Science Symposium*. SPIE, pp. 159–167. doi: 10.1117/12.2543437.
- Zylshal, Z. (2020) 'Topographic Correction of LAPAN-A3/LAPAN-IPB Multispectral Image : a Comparison of Five Different Algorithms', *Quaestiones Geographicae*, 39(3), pp. 33–45. doi: <https://doi.org/10.2478/quageo-2020-0021>.